Sensors & Transducers

Published by IFSA Publishing, S. L., 2016

http://www.sensorsportal.com

To Measure Relative Permittivity of Atmospheric Ice Using Frequency Sweep

[1] Umair N. Mughal and Beibei Shu

Arctic Technology Research Team, Institute of Industrial Technology,
UiT The Arctic University of Norway, 8505-Narvik, Norway

[1] Tel.: +47 76966372

[1] E-mail: umair.n.mughal@uit.no

Received: 25 July 2016 /Accepted: 30 September 2016 /Published: 31 October 2016

Abstract: The use of AD59333 IC for detecting atmospheric ice and atmospheric ice type was evaluated in this article. A prototype circuit was developed and was tested using a frequency sweep from 40 Hz to 20 kHz. The IC was calibrated using 100 kΩ resistor. The real and imaginary components of discrete Fourier transform were recorded at each frequency increment in order calculate the gain factor at each frequency increment. The unknown impedance was then calculated at each frequency increment. Results reflect that it was possible to use the dielectric loss data to detect an icing event and however it was difficult to determine icing type using AD5933 IC.

Keywords: AD5933, Atmospheric ice, Conductivity, Dielectric Constant, Dissipation factor, Frequency sweep.

1. Introduction

1.1. Capacitance Measurement Using Frequency Sweep

Capacitive ice sensors generate an electric field to detect the presence of dielectric materials. An electric field radiates outward around the probe and a dielectric material in close proximity of the field affects the measured capacitance. Capacitance $C = C_0\varepsilon_0\varepsilon_r$[1] can be measured by the variation in electrode geometry ‘C_0’ or by the variation in relative permittivity or dielectric constant ‘ε_r’.

Water molecule is polar in nature (Fig. 1a) due to electronegativity difference of 1.2 between hydrogen and oxygen. These polar molecules orient themselves with the electrical field, see Fig. 1c. However when the electrical field is removed they disorient themselves, Fig. 1b. Under the influence of electric field, polar molecule behave like a parallel combination of capacitor and resistor. The electrical current across this polar molecule can be defined,

$$I = I_c + I_l = Vj\omega C_0\varepsilon_0\varepsilon_r = V(j\omega C_0\varepsilon_0)(\varepsilon_r' - j\varepsilon_r'') \quad (1)$$

The constant $\varepsilon_r(\omega) = \varepsilon_r'(\omega) - j\varepsilon_r''(\omega)$ is the complex dielectric constant which is dependent upon the excitation frequency. Here ε_r' represents the amount of energy from the electric field which is stored in the material and ε_r'' represents how lossy or dissipative a material is to the external electric field. This loss factor $\varepsilon_r''(\omega)$ includes the effects of both dissipation and conductivity. Also the relative loss of

[1] $C_0 = A/d$ where A is the area of the electrode and d is the distance between the electrodes, ε_0 is the permittivity of vacuum equal to 8.85x10^{12} F/m.

the material is the ratio of energy lost to the energy stored and is defined as 'dissipation factor $D = tan\,\delta = \varepsilon_r''/\varepsilon_r'$. Polar materials generally have many dielectric mechanisms (atomic, electronic and dipolar) in different frequency domains associated with a cutoff frequency in each domain which appears as a peak in $\varepsilon_r'' = \varepsilon_r''(\omega)$ (likewise $D = D(\omega)$) curve. This dipolar orientation is generally associated with the relaxation[2] phenomenon, whereas the electronic and atomic polarization are associated with the resonance phenomenon. In the frequency domain analysis, the relaxation frequency 'f_c' is indicative of the relaxation time, $\tau_0 = 1/2\pi f_c$. This frequency can be detected by a peak by sweeping the excitation frequency and is generally unique for different materials. Due to variation in temperature the relaxation time follows Boltzmann distribution for thermal vibrations, $\tau = \tau_0 e^{H/kT}$, hence it is higher if the temperature is lower. Here H is the activation energy, k is the Boltzmann constant and T is the absolute material temperature. If we replace $\varepsilon(\omega \rightarrow 0) = \varepsilon_s$ and $\varepsilon(\omega \rightarrow \infty) = \varepsilon_\infty$, then by varying excitation frequencies, the dielectric constant of polar material can be analytically described by Debye relation, see Eq. (2) and Figs. 2a and 2b.

$$\varepsilon(\omega) = \varepsilon_\infty + \frac{\varepsilon_s - \varepsilon_\infty}{1 + j\omega\tau} \quad (2)$$

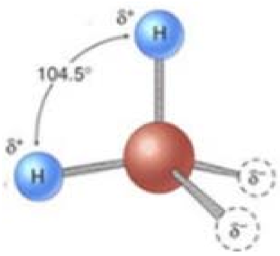

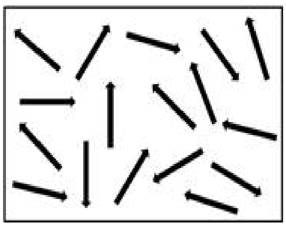

(a) Water Molecule, (b) Absence of electrical field.

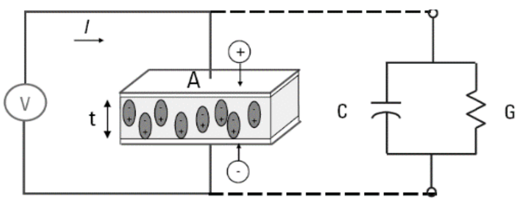

(c) Polar Molecule in an Electrical Field [1]

Fig. 1. Polar Material Electrical Characteristics.

1.2. Dielectric Constant of Atmospheric Ice

Fig. 2a shows the variation in dielectric constant variations of a sample of pure ice at two different temperatures ($-8\,^0C$ and $-15\,^0C$). Both curves of $\varepsilon_r'(\omega)$ and $\varepsilon_r''(\omega)$ are shifting towards left as temperature was decreasing. The relaxation frequency 'f_c' was in the range of $1 \rightarrow 10$ kHz where the value of $\varepsilon_r''(\omega)$ is in the range of $40 \rightarrow 50$. Also Fig. 2b shows the variation in dielectric constant variations of three distinct samples of snow with density ratios ρ= 0.095, 0.132 and 0.254.

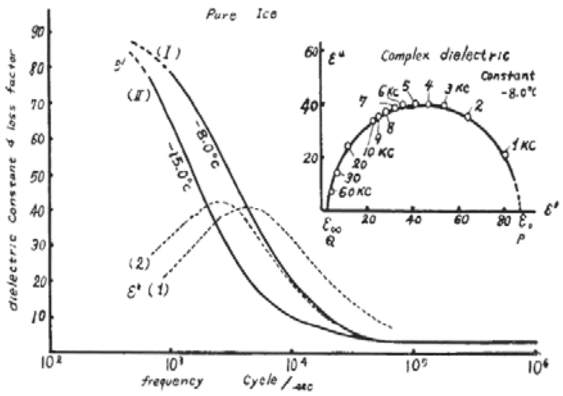

(a) ε_r variation of pure ice at two temperatures

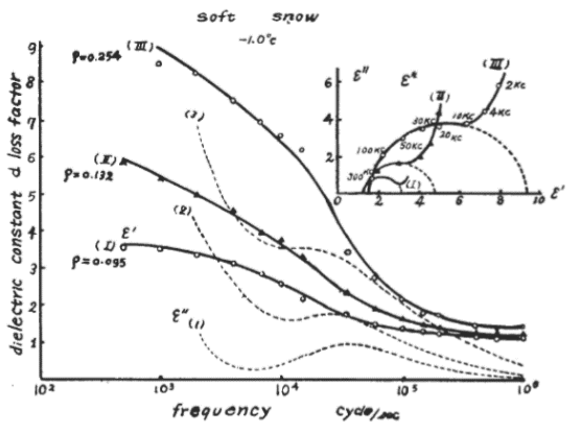

(b) ε_r variation of snow at three density ratio's

Fig. 2. Visualization of Debye Relations [5].

Both curves of $\varepsilon_r'(\omega)$ and $\varepsilon_r''(\omega)$ are increasing in magnitude as the desity ratio's are increasing. The low frequency deviation of these curves from the ideal semi circle behavior (in Argand Diagram) is due to the conductivity of snow which is increasing with increasing density ratio's. However the relaxation frequency 'f_c' was not quite distinct but it lie in the range of $10 \rightarrow 100$ kHz where the value of $\varepsilon_r''(\omega)$ are under 4 for all density ratio's. The application of the electrical properties to the measurement of ice thickness, temperature, crystal orientations are also presented in Evans [2]. It is mentioned in Sihvola et. al. [3] that for dry snow, the dielectric constant is determined by the density and for wet snow, the imaginary part and the increase of the real part due to

[2] Relaxation time τ_0 is a measure of the mobility of the dipoles that exist in the material to reorient themselves. For a pure material this relaxation time is unique.

liquid water have the same volumetric wetness dependence. In Sihvola et. al. [3], the results indicate that the complex dielectric constant is practically independent of the structure of snow. The static dielectric constants ε_{rs} of both polycrystalline and single crystals of ice have been carefully determined, Auty and Cole [4].

Weinstein [6] and Jarvinen [7] proposed two different capacitive based ice detection methods. Jarvinen in his patent [7] have proposed the use of AD5933 to detect icing event, icing type, ice thickness and icing rate. The capacitance measurement technique was also highlighted in state of the art review by Mughal et. al. [8] and Homola et. al. [9], who have categorize capacitance measurement technique to be one of the many possible measurement techniques to detect atmospheric icing event, icing type and icing rate.

1.3. AD5933 IC and its usage

AD5933 is a smallest and lowest power solution to measure the range of impedances using discrete Fourier components. The general impedance measurement system can be seen in Fig. 3. The system is excited by a range of frequencies and output phase and impedance magnitude is measured. This approach is called the frequency domain measurement technique [10].

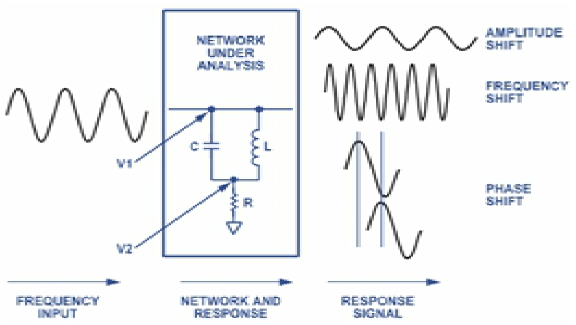

Fig. 3. General Impedance Measurement System [11].

In the block diagram Fig. 4, a direct digital synthesizer or DDS (AD9834) is used to generate a predefined frequency sweep to a tuning resolution of 0.1 Hz → 100 kHz. The output frequency is then filtered and amplified before being applied to the known impedance. ADC is then utilized to sample synchronously across all frequencies so as both the excitation and response waveform can be compared to allow full phase information. The data is then delivered to DSP for further processing. The functional block diagram of this IC could be seen in Fig. 5.

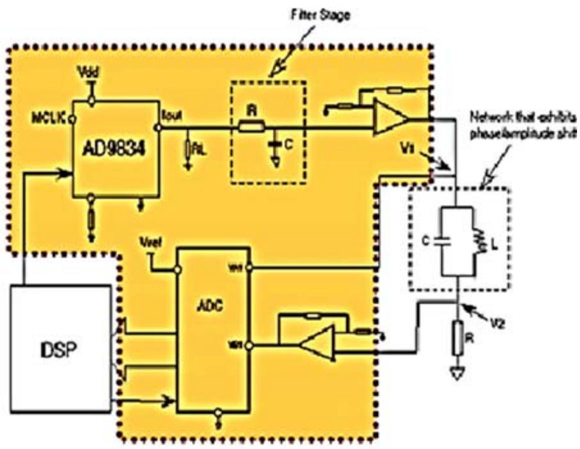

Fig. 4. Integrated single chip solution [11].

AD5933 IC have been utilized in impedance spectroscopy, proximity sensing, chemical analysis, bio medical analysis, human body impedance analysis and corrosion analysis. Norbotten B. J. [12] used AD5933 in the frequency range of 5 → 100 kHz and measured human body impedance in the range of 0.1 kΩ → 10 MΩ. Similarly Pena A. A. [13] developed spectrometer for electrical bioimpedance using this IC. Nevertheless this IC have also been utilized for measuring blood glucose levels by Kamat et. al. [14].

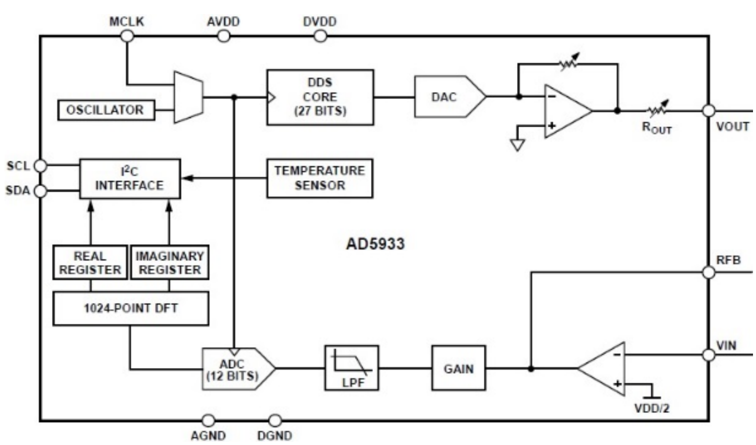

Fig. 5. Functional Block Diagram [15].

This article is an extended version of the Mughal and Shu [16] and is divided in four sections. Section 1 is an introduction which is further divided in three section in order to understand atmospheric ice capacitance measurement technique using frequency sweep approach and application/construction of AD5933 IC. Section 2 is about the approach and architecture of the circuit developed to measure capacitance of atmospheric ice. Section 3 describes the experimental results and discussions. Section 4 is the conclusion.

2. Approach & Architecture

The frequency generator allows an external complex impedance to be excited with a known frequency. The frequency generator require three inputs which are start frequency 'F_{START}', incremental frequency 'ΔF' and number of frequency increments 'N_{INCR}', see Fig. 6.

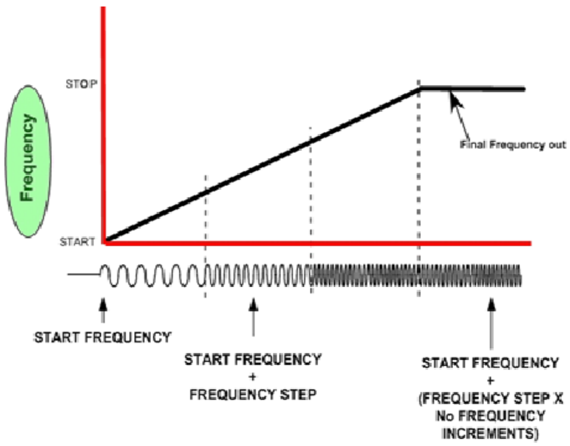

Fig. 6. Frequency sweep characteristics.

The microcontroller selected to implement the architecture was Atmega128 due to its memory. Also, this microcontroller had the flexibility to read/write on AD5933 IC's internal registers through I^2C interface nevertheless the I^2C address of AD5933 was fixed by the manufacturer. In this experiment it was desired to sweep the frequency from 40 Hz → 20 kHz for a step of 40Hz. In order to meet this requirement, a changeable clock signal for AD5933 IC, was generated through Atmega128 timer1 in CTC mode, see Fig. 7. In CTC mode the counter was cleared to zero, when the counter value (TCNT1) matches either the OCR1A (WGM13:0 = 4) or the ICR1 (WGM13:0 = 12). The counter value (TCNT1) was increased until a compare match occurs with either OCR1A or ICR1, and then counter (TCNT1) was cleared, see Fig. 8.

The function of timer1 over here was to generate frequencies, so that the CTC interrupt should be disabled to save CPU cycles. This AVR timer was connected to general I/O Port. Then general I/O pin PD5 was converted to compare match output OC1A. After that OC1A pin function was set to toggle on compare match. Then the fuse bits were programmed to make clock division factor to 1 and set the timer1 clock source to no prescaling. Hence the timer clock source was equal to crystal frequency, $clk_{I/O}$=11.0592 MHz. The output frequency was f_{out}= $clk_{I/O}/(2\times OCR1A)$. OCR1A was a 16-bits register, which ranged from 1 to 65535 therefore the range of output frequency could be was $clk_{I/O}/(2\times 1)$ to $clk_{I/O}/(2\times 65535)$, that is, from 5.5296 MHz to 84 Hz. Therefore when the system was running, the only requirement was to change the value of OCR1A to change the output frequency. Therefore using an internal clock source, which was 16.776MHz, the AD5933 chip could measure the impedance spectrum in the required frequency range of 1 kHz–100 kHz. However using external clock source (as applied in this work), which was generated by AVR, the frequency range can go lower than 1 kHz.

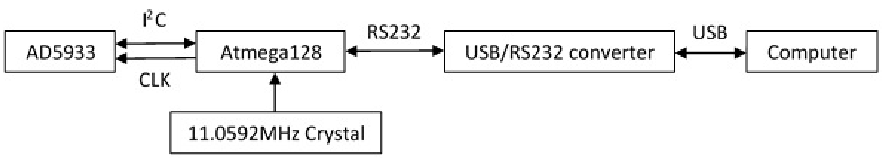

Fig. 7. Block diagram for communication path

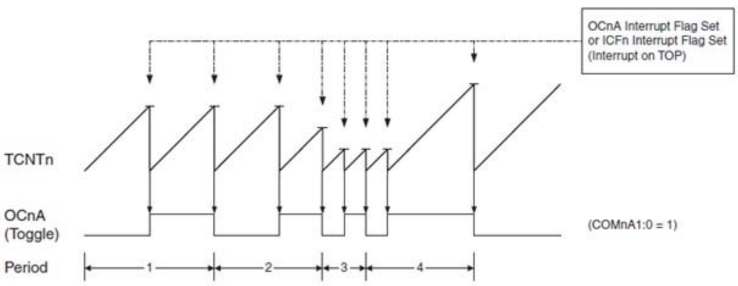

Fig. 8. CTC mode, timing diagram.

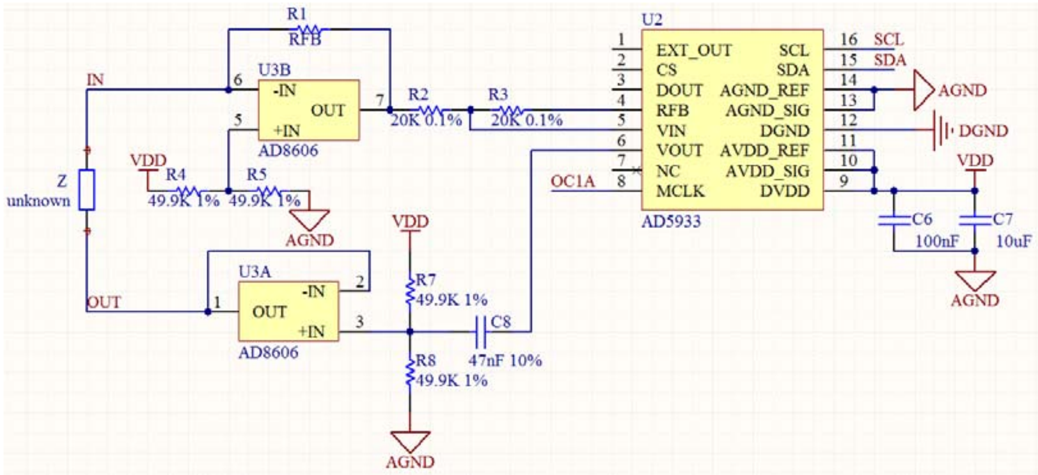

Fig. 9. Circuit Diagram for AD5933 Part.

This IC worked in two stages, which are transmit stage and receive stage. The transmit stage of the AD5933 was made up of a 27 bit phase accumulator DDS core which provided the output excitation signal at a particular frequency, see Fig. 10a. The input to the phase accumulator was taken from the contents of the start frequency register (Ram locations 82h, 83h and 84h). Although the phase accumulator offers 27bits of resolution, the start frequency register had the 3 most significant bits (MSBs) sets to 0 internally; therefore it became possible to program only the lower 24bits of the start frequency register. The frequency resolution 0.1Hz could be achieved. The frequency resolution was programmed via a 24 bit word loaded serially over the I^2C interface to the frequency increment register. The last input was number of increments

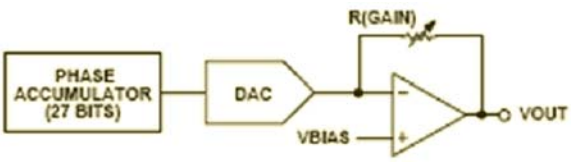

(a). Transmit Stage

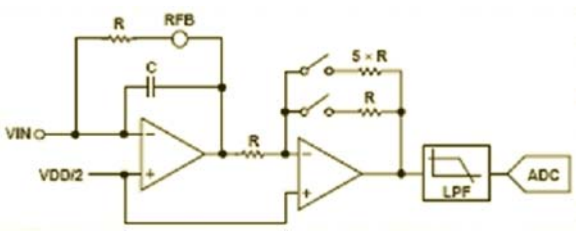

(b). Receive Stage

Fig. 10. Transmit Stage and Receive Stage of AD5933 [11].

The receive stage comprised of a current to voltage amplified, followed by a programmable gain amplifier (PGA), an anti aliasing filter, and an ADC, see Fig. 10b. The unknown impedance was connected between the V_{OUT} and V_{IN} pins. The first stage current to voltage amplifier sat the V_{IN} pin as a virtual ground with a DC value of $V_{DD}/2$. The signal current developed across the unknown impedance was then flowed into the V_{IN} pin which, developed a voltage signal at the output of the current to voltage converter.

The gain of the current to voltage amplifier was determined by selecting a feedback resistor of $Z_{calibrated} = 100k\Omega$ connected between RFB and V_{IN}. The aim was to maintain the signal within the linear range of ADC (0V to 3.3V AVDD). The gain setting was set to one. The signal was then send through a low pass filter and was presented to the input of the 12bit, 1MSPS ADC.

The response signal from the impedance was sampled by the on-board ADC and DFT processed by an on-board DSP engine. The DFT algorithm returned real 'R' and imaginary 'I' data-word at each frequency point along the frequency sweep. Using these 'R' and 'I', magnitude 'M' and phase 'φ' were calculated using (3) and (4) [1]. Therefore $M_{calibrated}$ and $\varphi_{calibrated}$ were measured using $R_{calibrated}$ and $I_{calibrated}$. Atmospheric ice was then placed on the electrode for which $M_{unknown}$ and $\varphi_{unknown}$ were measured using $R_{unknown}$ and $I_{unknowm}$.

$$M = \sqrt{R^2 + I^2}, \quad (3)$$

$$\varphi = tan^{-1}(I/R) \quad (4)$$

It was also necessary to ensure that the signal always maintained within the linear range of the ADC over the impedance range of interest. Before measuring the unknown impedance, the calibration

[1] R is the real number stored at Register Address 0x94 and Register Address 0x95. I is the imaginary number stored at Register Address 0x96 and Register Address 0x97.

must be done. In calibration stage, the manufacturer mentioned that a gain factor need to be calculated. The gain factor 'GF' could be calculated using,

$$GF = \frac{1}{Z_{calibrated} \times M_{calibrated}} \quad (5)$$

However in this analysis, there was no need to calculate the gain factor due to the reason that in the measuring stage, the unknown impedance '$Z_{calibrated}$' and its unknown phase were calculated using,

$$Z_{unknown} = \frac{Z_{calibrated} \times M_{calibrated}}{M_{unknown}} \quad (6)$$

$$\emptyset_{unknown} = atan\left(\frac{I_{unknown}}{R_{unknown}}\right) - atan\left(\frac{I_{calibrated}}{R_{calibrated}}\right) \quad (7)$$

As capacitance $C = 1/2\pi jfZ$, therefore using (6) and *(7)* in (1), we derive,

$$\varepsilon_r' - j\varepsilon_r'' = \frac{1}{2\pi jfC_0\varepsilon_0 Z_{unknown} exp(\emptyset_{unknown})} \quad (8)$$

Eq. (8) is utilized to determine the dielectric constant of the unknown sample of atmospheric ice.

3. Experimental Results and Discussions

Using Eq. *(*8), the results of ε_r' and ε_r'' were obtained by writing a simple algorithm in MatLab. The experimentations were done in the Cold Climate Chamber of UiT Campus Narvik, using following samples at the respective temperatures,

i. Glaze ice frozen on the electrode plate at a temperature of -16 °C;
ii. Glaze ice frozen on the electrode plate at a temperature of -20 °C;
iii. Glaze ice frozen on the electrode plate at a temperature of -24 °C;
iv. Natural Snow from ground outside university campus at a temperature of -3 °C;
v. Normal tap water at a temperature of 26 °C.

The results of glaze ice at three different temperatures could be seen in Fig. 11.

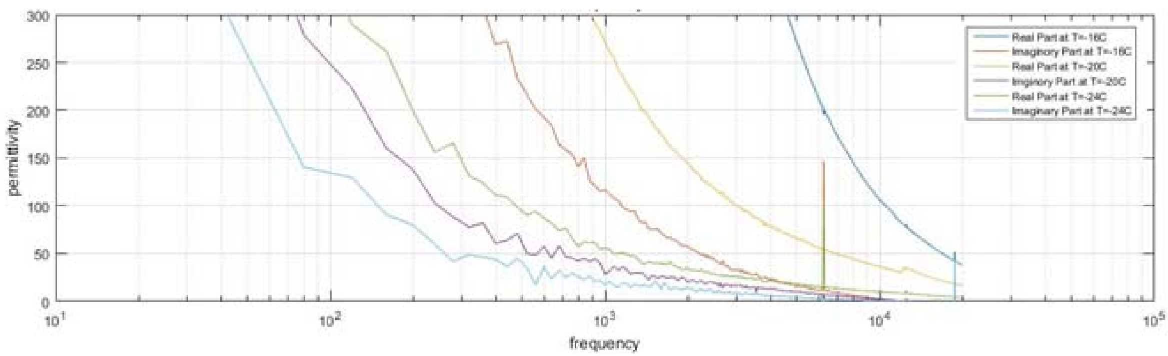

(a) Dielectric constant ($\varepsilon_r' = real, \varepsilon_r'' = imaginary$) variation with frequency

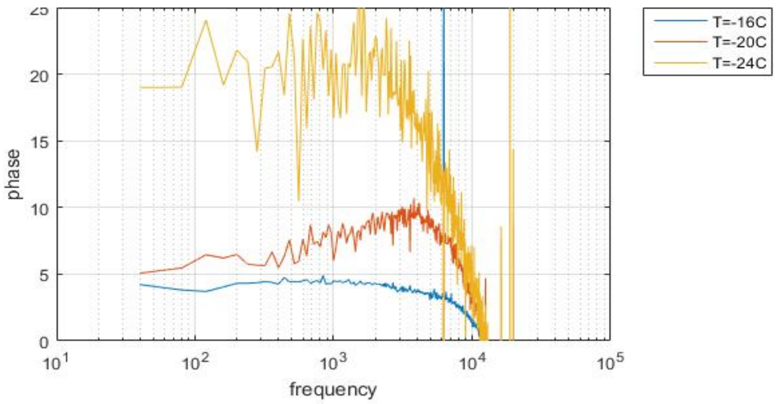

(b) Dielectric constant phase (atan($\varepsilon_r''/\varepsilon_r'$))

Fig. 11. Dielectric constant variation with excitation frequency for Glaze Ice frozen on the electrode plate at temperatures -16 ºC, -20 ºC and -24 ºC [18].

This figure indicate there was no prominent peak observed in the dielectric constant variation (ε_r'' = imaginary part) with the variation in frequency (Fig. 11a), hence it was not possible to compare the results of Stiles [5] and Kuroiwa [17]. Both curves of $\varepsilon_r'(\omega)$ and $\varepsilon_r''(\omega)$ were shifting towards left as temperature was decreasing. However the capacitance phase ($atan(\varepsilon_r''/\varepsilon_r')$)[1] or dissipation factor ($\varepsilon_r''/\varepsilon_r'$) reflect observable trend. In the frequency range of $1 \rightarrow 10$kHz (relaxation frequency 'f_c'), the variation in the phase is prominent (Fig. 11b). This value of f_c was found in agreement with the experimental results of Stiles (Fig. 2). It was also found that that the average value of this phase reached to a relative maximum of 20^0 by decreasing the temperature from $-16\,^0C \rightarrow -24\,^0C$, hence more capacitance. The results were however very noisy due to high conductance of atmospheric ice. The argand diagram was also not forming a semi circle due to very high conductance at low frequencies. In another test, the results were compared with the natural occurring snow, collected from outside the university campus and water samples. The results are shown in Fig. 12. These results also indicated the same trend in the dielectric constant variation (ε_r'' = imaginary part) with frequency (Fig. 12a), hence it was not possible to determine the relaxation due to very high conductivity values. Similarly it was found that the phase of the capacitance ($atan(\varepsilon_r''/\varepsilon_r')$) reflect observable trend for samples of glaze ice, snow and water (Fig. 12b).

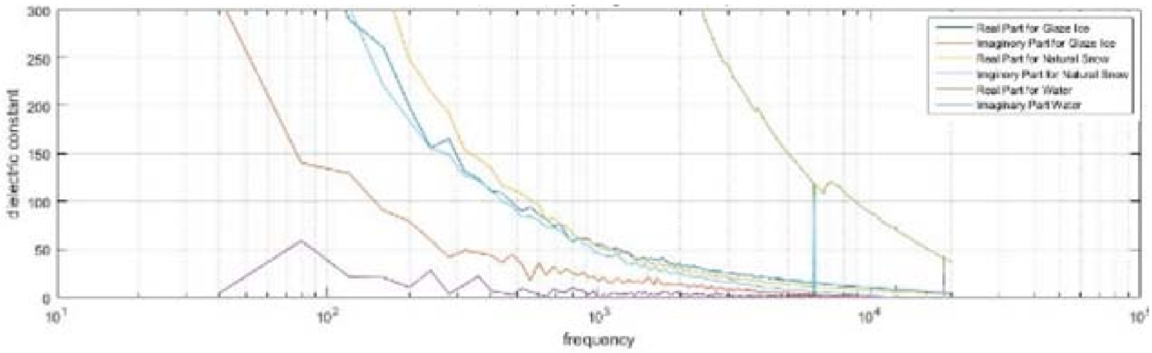

(a) Dielectric constant ($\varepsilon_r' = real, \varepsilon_r'' = imaginary$) variation with frequency

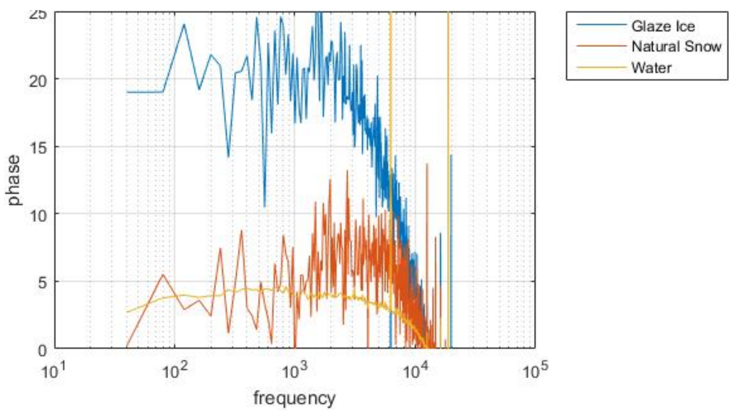

(b) Dielectric constant phase (atan($\varepsilon_r''/\varepsilon_r'$))

Fig. 12. Dielectric constant variation with excitation frequency for glaze ice at -24 °C, natural snow at -4 °C and water sample at 24 °C [18] Conclusions.

AD5933 IC works upon the frequency domain capacitance measurement technique [10]. It is possible to use the capacitance phase or dissipation factor for detecting an icing event. Most of the existing experimental study ([2, 5, 17]) by sweeping the frequency to determine the dielectric variation in different type of atmospheric ice are laboratory based. However the aim in this article was to propose an atmospheric icing sensory solution using AD5933 IC. It is therefore found that using AD5933 IC to detect an atmospheric event is possible however to detect the type of atmospheric ice would be difficult to achieve using this IC due to the conductivity of ice sample.

Acknowledgment

The work was funded by Research Council of Norway Project No. 195153 (ColdTech RT3), Norwegian Centre for International Cooperation in Education Project No. HNP-2014/10023 and WindCoE (Nordic Wind Energy Centre) project

[1] Capacitance phase is analogous to dissipation factor $D = \tan\delta = \varepsilon_r''/\varepsilon_r'$

funded within Interreg IVA Botnia-Atlantica, as part of European Territorial Cooperation (ETC).

References

[1]. Basics of measuring dielectric properties of materials. Agilent. (March 14th). Available: http://cp. literature. agilent.com/litweb/pdf/5989-2589EN.pdf

[2]. S. Evans, Dielectric properties of ice and snow - a review, *Journal of Glaciology*, Vol. 5, 1965, pp. 773-792.

[3]. A. Sihvola, E. Nyfors, and M. Tiuri, Mixing formulae and experimental results for the dielectric constant of snow, *Journal of Glaciology*, Vol. 31, 1985, pp. 163-170.

[4]. R. P. Auty and R. H. Cole, Dielectric Properties of Ice and Solid D_2O, *Journal of Chemical Physics*, Vol. 20, 1952, pp. 1309-1314.

[5]. W. H. Stiles and F. T. Ulaby, Dielectric properties of snow, *Journal of Geophysical Research*, Vol. 85, 1981, pp. 91-103.

[6]. L. M. Weinstein, Ice Sensor, *US Patent 4766369*, 1988.

[7]. P. O. Jarvinen, Total impedance and complex dielectric property ice detection system, *US Patent 7439877 B1*, 2008.

[8]. U. N. Mughal, M. S. Virk, and M. Y. Mustafa, State of the Art Review of Atmospheric Icing Sensors, *Sensors & Transducers*, Vol. 198, Issue 3, March 2016, pp. 2-15.

[9]. M. C. Homola, P. J. Nicklasson, and P. A. Sundsbo, Ice sensors for wind turbines, *Cold Regions Science and Technology*, Vol. 46, 2006, pp. 125-131.

[10]. K. Kao, Dielectric Phenomena in Solids, *Elsevier*, 2004.

[11]. AD5933 Impedance to Digital Converter, *Analog Devices*, 2016, http://dkc1.digikey.com/us/en/TOD/ADI/AD5933/AD5933.html

[12]. B. J. Nordbotten, Bioimpedance Using the Integrated Circuit AD5933, Master of Science, Department of Physics, *University of Oslo*, 2008.

[13]. A. A. Pena, A Feasibility Study of the Suitability of an AD5933 based spectrometer for EBI Applications, Electronic Instrumentation, *University of Boras*, 2009.

[14]. D. K. Kamat, B. Dhanashri, and P. M. Patil, Blood Glucose Measurement Using Bioimpedance Technique, *Advance in Electronics*, Vol. 2014, 2014.

[15]. Datasheet AD5933. *Analog Devices*, 2016, Available: http://www.analog.com/media/en/technical-documentation/data-sheets/AD5933.pdf

[16]. U. N. Mughal and B. Shu, Using AD5933 IC To Measure Dielectric Constant Variation of Atmospheric Ice, in *Proceedings of the 10th International Conference on Sensor Technologies and Applications (SENSORCOMM'16)*, Niece, France, 24-28 July 2016, pp. 34-39.

[17]. D. Kuroiwa, The dielectric property of snow, *Union Geodesique et Geophysique International*, Association Internationale of Hydrologie Scientifique, Assemblee generale de Rome, 1956, pp. 52-63.

[18]. U. N. Mughal, B. Shu, and T. Rashid, Proof of Concept of Atmospheric Icing Sensor to detect icing, determine icing type and measure melting rate, *Submitted in IEEE Transactions on Dielectrics and Electical Insulation, Paper ID 6048*, 2016.